

Single-Molecule Imaging of an *in Vitro*-Evolved RNA Aptamer Reveals Homogeneous Ligand Binding Kinetics

Mark P. Elenko,[†] Jack W. Szostak,[‡] and Antoine M. van Oijen^{*§}

Program in Biological and Biomedical Sciences, Harvard Medical School, 25 Shattuck Street, Boston, Massachusetts 02115, Howard Hughes Medical Institute and Center for Computational and Integrative Biology, Massachusetts General Hospital, 185 Cambridge Street, Boston, Massachusetts 02114, and Department of Biological Chemistry and Molecular Pharmacology, Harvard Medical School, 240 Longwood Avenue, Boston, Massachusetts 02115

Received March 10, 2009; E-mail: antoine_van_oijen@hms.harvard.edu

Aptamers are nucleic acid molecules that bind ligands with high specificity and affinity. Aptamers for a wide array of targets have been found by *in vitro* selection experiments,¹ and natural aptamers in the form of riboswitches have also been discovered.² In addition to their value as possible tools and therapeutics,^{3,4} these molecules are of great interest as a means of gaining insight into the relationships between molecular complexity, structure, and functional ability.⁵ Aptamer binding has previously been investigated using bulk ensemble-averaging approaches, making it challenging to identify heterogeneous behavior within populations of molecules with a single defined sequence and essentially impossible to study the functional heterogeneity of evolving populations or random-sequence libraries. To address this problem, we have developed a single-molecule imaging approach for exploring the functional heterogeneity of *in vitro*-evolved RNA aptamers. Single-molecule techniques have proven to be especially fruitful for work on functional RNA, illuminating the dynamics of phenomena that occur on time scales from milliseconds to minutes, such as folding, conformational change, and catalysis.⁶ Here we report single-molecule studies of RNA aptamer binding kinetics on time scales of minutes to days. In an investigation of an aptamer evolved and optimized by *in vitro* selection, we found great uniformity in its small-molecule binding kinetics, a notable contrast to the heterogeneity observed for the folding kinetics of some natural ribozymes.⁷

We imaged the binding of a fluorescently labeled guanosine triphosphate (GTP) ligand to single molecules of the Class V aptamer, an RNA aptamer previously found by *in vitro* selection and optimized for a 235-fold improvement of affinity.^{5,8,9} Class V displays an affinity of 17 nM for GTP with slow on and off rate constants [see the Supporting Information (SI)]. The aptamer was annealed to a biotinylated DNA oligonucleotide and coupled to a streptavidin-coated surface incorporated into a microfluidic flow cell (Figure 1A; see the SI for detailed methods). GTP was labeled at the γ -phosphate with tetramethylrhodamine (TMR), and the K_d of the aptamer for the GTP–TMR conjugate was 0.5 nM (see the SI). GTP–TMR was introduced into the flow cell at a concentration of 300 pM. We used total internal reflection fluorescence (TIRF) microscopy¹⁰ to image the fluorescence of aptamer-bound GTP–TMR on a CCD camera. With a field of view of $85 \times 85 \mu\text{m}^2$ and a surface density of ~ 0.4 aptamer/ μm^2 , we visualized hundreds of individual active aptamers in a field. Binding of the labeled GTP ligand to immobilized aptamers is observable as the appearance of single bright spots (Figure 1B). Nonbinding (misfolded) aptamers are not detected.

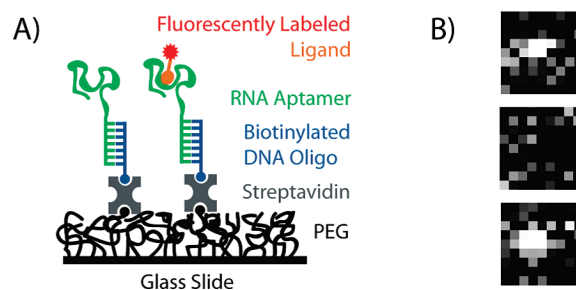


Figure 1. Experimental design. (A) Schematic depiction of aptamer immobilization on a functionalized surface. (B) Example of fluorescence images visualizing binding of a fluorescent GTP to an aptamer (top), dissociation (middle), and rebinding of another labeled ligand (bottom).

To determine the on and off rates for individual aptamer molecules, we needed to observe many ligand-binding events per aptamer, which required acquisition times of thousands of minutes (multiple days). These acquisition times are several orders of magnitude longer than the norm for single-molecule assays and necessitated the development of novel methods. Fluorescence images were acquired at regular intervals (every 2 min for Class V) using a shuttered laser, stretching the fluorophore lifetime over a long period in order to minimize the probability of photobleaching of bound GTP–TMR. An enzymatic oxygen-scavenging system¹¹ was employed and the solution periodically refreshed, helping to reduce RNA photodamage (see the SI). Automated image-analysis routines were used to correct for lateral stage drift and, most crucially, to eliminate focal drift (see the SI). Automated particle-finding algorithms were used to locate bright spots and extract their intensities as a function of time. The resultant single-molecule time–intensity traces showed the characteristic telegraph-like nature corresponding to repeated binding and dissociation of fluorescently labeled ligand by a single aptamer, allowing the identification of on events (fluorescent ligand bound to the aptamer) and off events (no fluorescent ligand) (Figure 2A).

Measuring the on and off event times allowed us to produce distributions of event durations containing information on the association and dissociation rate constants. For the Class V aptamer, both the aggregated and individual-molecule event distributions were well-fit by single-exponential curves (Figure 2B), yielding single on and off rates (and thus the equilibrium dissociation constant). Analyzing the event duration distributions for each aptamer molecule ($N = 103$) provided us with distributions of single-molecule on and off rate constants (Figure 3A), which yielded a K_d estimate of 0.28 nM, a close match to the value found by bulk fluorimetry (see the SI). The shape and width of the on-event distribution can be explained entirely by the uncertainty in determining a rate by sampling a limited number of

[†] Program in Biological and Biomedical Sciences, Harvard Medical School.

[‡] Massachusetts General Hospital.

[§] Department of Biological Chemistry and Molecular Pharmacology, Harvard Medical School.

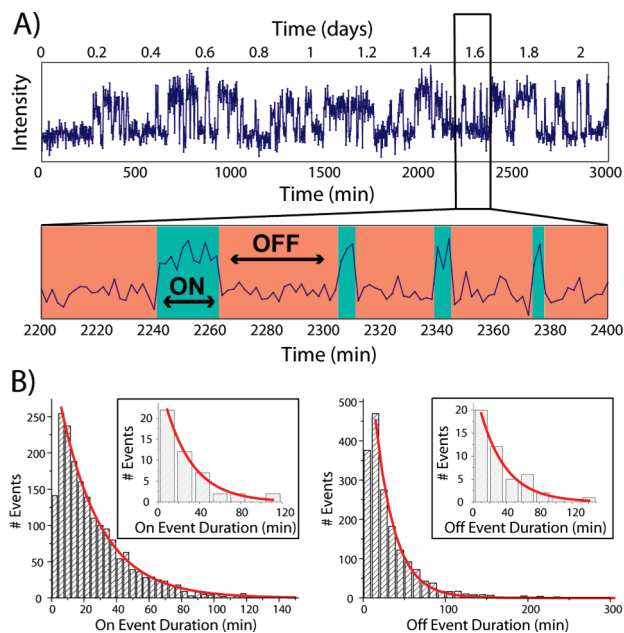


Figure 2. Event analysis. (A) Fluorescence intensity trajectory of the particle depicted in Figure 1B. On and off events are denoted by green and red, respectively. (B) Histograms of all on and off events detected in the trajectories of a large number ($N = 103$) of single-aptamer traces. Insets show event distributions from the single trajectory shown in Figure 2A.

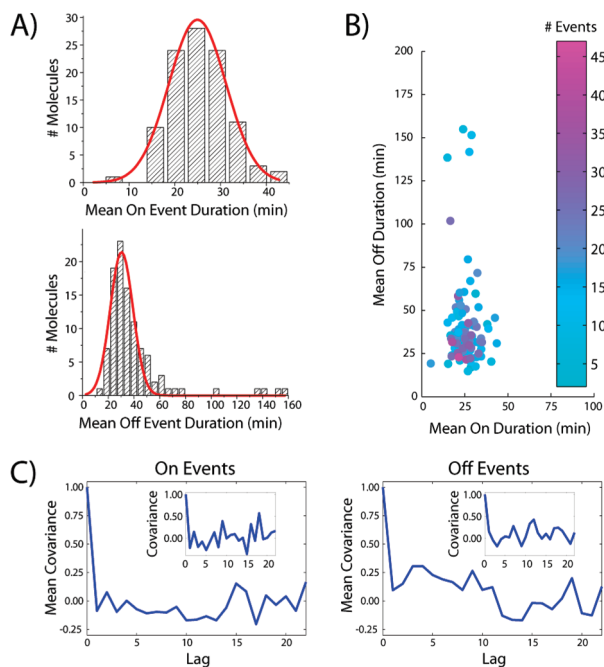


Figure 3. Single-molecule analysis results. (A) Histograms of the average on and off times for individual single-aptamer traces. (B) Scatter plot of the mean on and off durations obtained from individual single-aptamer trajectories. (C) Average autocorrelation functions of the on- and off-event durations. Insets show autocorrelations for the single-aptamer trajectory from Figure 2A.

events; this is also the case for the off-event distribution when an outlying $\sim 3.4\%$ of the events are removed (see the SI). On average, zero or one of these outlying off events were found in each trajectory. This small deviation may have been caused by unseen on events produced by unlabeled or dim ligand or by missed short on events, thus giving rise to false long off events. Experiments with a short (500

ms) time interval yielded only single-rate on-event distributions commensurate with photobleaching, suggesting that no binding kinetics occur on faster (second) time scales (see the SI). Single-molecule rate constants can be used to visualize the population of molecules in a “kinetic space” (Figure 3B). The tight localization made possible by the observation of many events allows for sensitive detection of functional heterogeneity within populations of molecules of a given sequence or within the heterogeneous populations from directed-evolution experiments. This could be extended by RNA labeling to capture currently unmonitored folding heterogeneity.

The single-molecule analysis provides information on temporal variations not accessible by ensemble methods. We analyzed the temporal dynamics of individual aptamers by calculating autocorrelation coefficients (Figure 3C). The autocorrelation function (see the SI) is a very sensitive measure of molecular-state memory. The averaged autocorrelations tend toward zero for all lags, implying that Class V has no memory, unlike some more complex systems, such as certain protein enzymes.^{12,13} Correlation histograms also show no evidence of memory (see the SI). These data suggest that the binding-competent RNA is not subject to conformer exploration on a kinetically relevant time scale. The maintenance of stable or highly favored binding-competent folding is consistent with the proposal that the affinity of tightly binding aptamers is determined by high structural stability.^{9,14}

In vitro selections explore large heterogeneous pools, typically on the order of 10^{15} initial random sequences, searching for functional sequences (such as aptamers) through iterated cycles of amplification and selection. Unfortunately, this process distorts and obscures the true distribution of functionality in the original sample of sequence space. Single-molecule imaging over long time scales offers the dynamic range needed to permit the direct analysis of distributions of kinetic properties in such pools. Single-molecule methods may therefore provide a means of delving into a fundamental biochemical question: the nature of the relationship between biopolymer information and function.

Acknowledgment. Dr. A. Luptak provided initial assistance, and Dr. A. Ricardo helped perform compound characterization. J.W.S. is an investigator of the Howard Hughes Medical Institute.

Supporting Information Available: Materials and methods; aptamer affinity, rates, and specific binding; RNA photodamage; data processing and analysis; and a movie (AVI). This material is available free of charge via the Internet at <http://pubs.acs.org>.

References

- (1) Wilson, D. S.; Szostak, J. W. *Annu. Rev. Biochem.* **1999**, *68*, 611–647.
- (2) Montange, R. K.; Batey, R. T. *Annu. Rev. Biophys.* **2008**, *37*, 117–133.
- (3) Mairal, T.; Ozalp, V. C.; Lozano Sanchez, P.; Mir, M.; Katakis, I.; O’Sullivan, C. K. *Anal. Bioanal. Chem.* **2008**, *390*, 989–1007.
- (4) Lee, J. F.; Stovall, G. M.; Ellington, A. D. *Curr. Opin. Chem. Biol.* **2006**, *10*, 282–289.
- (5) Carothers, J. M.; Oestreich, S. C.; Davis, J. H.; Szostak, J. W. *J. Am. Chem. Soc.* **2004**, *126*, 5130–5137.
- (6) Zhuang, X. *Annu. Rev. Biophys. Biomol. Struct.* **2005**, *34*, 399–414.
- (7) Ditzler, M. A.; Aleman, E. A.; Rueda, D.; Walter, N. G. *Biopolymers* **2007**, *87*, 302–316.
- (8) Davis, J. H.; Szostak, J. W. *Proc. Natl. Acad. Sci. U.S.A.* **2002**, *99*, 11616–11621.
- (9) Carothers, J. M.; Oestreich, S. C.; Szostak, J. W. *J. Am. Chem. Soc.* **2006**, *128*, 7929–7937.
- (10) Axelrod, D. *Methods Enzymol.* **2003**, *361*, 1–33.
- (11) Aitken, C. E.; Marshall, R. A.; Puglisi, J. D. *Biophys. J.* **2008**, *94*, 1826–1835.
- (12) Lu, H. P.; Xun, L.; Xie, X. S. *Science* **1998**, *282*, 1877–1882.
- (13) Yang, H.; Luo, G.; Karnchanaphanurach, P.; Louie, T. M.; Rech, I.; Cova, S.; Xun, L.; Xie, X. S. *Science* **2003**, *302*, 262–266.
- (14) Carothers, J. M.; Davis, J. H.; Chou, J. J.; Szostak, J. W. *RNA* **2006**, *12*, 567–579.

JA901880V